Journal of Organometallic Chemistry 893 (2019) 1–10

Contents lists available at ScienceDirect

Journal of Organometallic Chemistry

journal homepage: www.elsevier.com/locate/jorganchem

Immobilization of Cu(II) on MWCNTs@L-His as a new high efficient reusable catalyst for the synthesis of pyrido[2,3-*d*:5,6-*d*′]dipyrimidine derivatives

Hakimeh Saeidiroshan, Leila Moradi*

Department of Organic Chemistry, Faculty of Chemistry, University of Kashan, Kashan, Iran

ARTICLE INFO

Article history:
Received 8 March 2019
Received in revised form
18 April 2019
Accepted 23 April 2019
Available online 29 April 2019

Keywords:
Multi-walled carbon nanotubes
Pyrido[2,3-*d*:5,6-*d*′]dipyrimidines
Organometallic catalyst
MWCNTs@L-His/Cu(II)
Reusable catalyst

ABSTRACT

In this research, a new heterogeneous organometallic catalyst was prepared through Cu(II) Immobilization on L-Histidine Functionalized multi-walled carbon nanotubes (MWCNTs@L-His/Cu(II)). Catalyst was prepared using a simple method and characterized by Fourier transform infrared (FTIR), scanning electron microscopy (SEM), Transmission electron microscopy (TEM), energy dispersive spectroscopy (EDS), thermal analysis (TGA), inductively coupled plasma optical emission spectrometry (ICP-OES) and Brunauer Emmett Teller (BET) techniques. A clean, rapid and efficient synthesis of pyrido[2,3-*d*:5,6-*d*′] dipyrimidine derivatives was accomplished in high to excellent yields and short reaction times *via* one-pot three-component condensation reaction of barbituric acid or 1,3-dimethylbarbituric acid, 6-aminouracil and aromatic aldehydes in the presence of MWCNTs@L-His/Cu(II) under reflux conditions. This new catalyst can be easily separated from the reaction mixture and recovered several times without a significant loss of activity.

1. Introduction

Multi-walled carbon nanotubes (MWCNTs) have attracted considerable interests due to their remarkable thermal conductivity [1,2], mechanical [3,4], and electrical properties [5–7]. In addition, their excellent chemical and mechanical stability and large surface area make them an ideal and potentially useful choice for applications in novel sensors [8], solar cells [9], optics [10], catalysis [11–13], polymer composites [14], and many others [15]. In recent years, CNTs has attracted tremendous attention as a catalyst support material for removing heavy metal ions such as lead [16], nickel [17], cadmium [18], copper [19], chromium [20] and other organic pollutants [21]. Without surface modification, most of CNTs lack sufficient binding sites for anchoring precursor metal ions or metal nanoparticles, which usually lead to poor dispersion and aggregation of metal ions, especially at high loading conditions. Therefore, the graphitic surface of nanotubes must be activated with functional groups to provide binding sites for coordination chemistry [22] such as other modified and applicable catalysts [23–25]. Histidine (2-amino-3-(4-imidazolyl)-propanoic acid) is an essential amino acid for human growth and repair of tissues and acts as a neurotransmitter in the central nervous of mammals [26]. The imidazole side chain of histidine can serve as a coordinating ligand in the metal ions transmission in biological bases and was detected in the active sites of certain enzymes [27,28]. Immobilization of L-Histidine/Cu(II) on to solid surfaces is the key step for creating a recoverable and reusable catalyst. The main advantage of this catalytic system is high surface area and low toxicity, potential towards applications in various fields such as uses in disciplines including physics, biomedicine, biotechnology, material science and catalysts.

Pyridopyrimidine derivatives are an important class of annulated uracils with broad range of biological, medicinal, and pharmacological properties that have attracted considerable interest in recent years [29,30]. Numerous reports delineate the antitumor [31], antiallergic [32], antioxidant [33], antifungal [34], antimicrobial [35], antibacterial [36] and antiviral activities [37] of these compounds.

The synthesis of pyrido[2,3-*d*:5,6-*d*′]dipyrimidine is carried out with various catalysts such as piperidine [38], triethanol amine [39], $Zr(H_2SO_4)_4$ [40], SBA-Pr-SO_3H [41], PTSA [42] and P_2O_5 [43]. Some of these protocols have their own merits and demerits, such as low yields of products, long reaction times, harsh reaction

* Corresponding author.
E-mail address: l_moradi@kashanu.ac.ir (L. Moradi).

https://doi.org/10.1016/j.jorganchem.2019.04.023
0022-328X/

conditions and tedious work-ups leading to the generation of toxic waste. Therefore, a great deal of effort is being directed to developing an efficient catalytic system for the synthesis of pyrido[2,3-d:5,6-d']dipyrimidine.

In this article, we decided to investigate the application of L-Histidine/Cu(II) complex immobilized on MWCNTs surfaces (MWCNTs@L-His/Cu(II)) as a highly efficient and reusable catalyst for the synthesis of pyrido[2,3-d:6,5-d']dipyrimidine derivatives *via* one-pot three-component condensation reaction of barbituric acid or 1,3-dimethylbarbituric acid, 6-aminouracil and aromatic aldehydes under reflux conditions (Scheme 1).

2. Experimental

2.1. Materials and apparatus

MWCNTs were purchased from Shenzhen Nanotechnologies China. The Purity of the CNTs was about 90–95% and the diameters and lengths ranging are between 20 and 40 nm and 5–15 μm respectively. Also, all organic materials were obtained commercially from the Sigma-Aldrich and Merck and were used without further purification. FT-IR spectra were obtained as KBr pellets on a PerkinElmer 781 spectrophotometer and on an impact 400 Nicolet FT-IR spectrophotometer. ^{1}HNMR and ^{13}CNMR spectra were recorded with DMSO-d_6 solution and tetramethylsilane as internal standard on a Bruker DRX-400 spectrometer for (^{1}H) and Bruker DRX-250 spectrometer for (^{13}C). Thermogravimetric analysis (TGA) was performed on a mettle TA4000 system TG-50 at a heating rate of 10 K min^{-1} under N_2 atmosphere. Scanning electron microscopy (SEM) images were obtained on LEO-1455VP equipped with an energy dispersive X-ray spectroscopy. Transmission electron microscopy (TEM) micrographs were recorded by a Philips CM120 instrument. The energy dispersive spectrometry (EDS) analysis was studied by XL30, Philips microscope. All sonication processes were accomplished by an ultrasonic bath (UA03MFD, Fungi Ultrasonic) with a frequency of 40 kHz and power of 80 W. Elemental analyses of the catalyst with inductively coupled plasma optical emission spectroscopy (ICP-OES) were obtained from an ICP-OES simultaneous instrument (VISTA-PRO). Melting points were measured with a Yanagimoto micro-melting point apparatus. Brunauer Emmett Teller (BET) analysis was used to determine the surface area of catalyst by Microtrac BEL Corp instrument and the purity determination of the substrates and reaction monitoring were accomplished by TLC on silica-gel Polygram SIL G/UV 254 plates (from Merck Company).

2.2. Preparation of catalyst

2.2.1. Preparation of MWCNTs-OH

Raw MWCNTs (0.2 g) and 100 ml methylene chloride were added into a 250 ml flask, and the mixture was dispersed by ultrasonication for 10 min. SDS (0.2 g) being dissolved in 10 ml H_2O, 10 ml acetic acid and $KMnO_4$ solution (0.25 g $KMnO_4$ dissolved in 5 ml H_2O) were added to the flask. The mixture was stirred vigorously at 25 °C for 24 h. After that, the mixture was filtered and washed with HCl and methanol and dried in an oven at 85 °C for 8 h.

2.2.2. Preparation of MWCNTs-CPTES

In order to prepare MWCNTs-CPTES, 1 g of MWCNTs-OH was added to 1 ml (5 mmol) CPTES (3-chloropropyl-triethoxysilane) dissolved in 100 ml dried toluene and the mixture was dispersed by ultrasonication. After this stage, the mixture was stirred for 18 h at 60 °C. Obtained MWCNTs-CPTES was washed with toluene and dried in an oven at 85 °C for 8 h.

2.2.3. Preparation of MWCNTs@L-Histidine

In the next step, MWCNT-CPTES (1 g) was dispersed in 100 ml deionized water followed by sonication for 20 min, and then L-Histidine (2 g) was added to the mixture and stirred at 90 °C for 15 h under N_2 atmosphere. The product was separated by filtration and washed several times with distilled water to remove the unattached substrates and dried in an oven at 85 °C for 8 h.

2.2.4. Preparation of MWCNTs@L-His/Cu(II)

In last step of catalyst preparation, MWCNTs@L-His was used as the support and ligand for entrapment of Cu(II). In this procedure, the synthesized MWCNTs@L-His (1 g) was dispersed in absolute ethanol (30 ml) for 20 min and $Cu(NO_3)_2$ $3H_2O$ (0.5 g) was added to the mixture and refluxed for 24 h. Then, the reaction mixture was cooled to room temperature and the final product was separated with filtration, washed with ethanol and dried in an oven at 85 °C for 8 h.

2.3. General procedure for the synthesis of pyrido[2,3-d:5,6-d'] dipyrimidine derivatives using MWCNTs@L-His/Cu(II)

A mixture of barbituric acid or 1,3-dimethylbarbituric acid (1 mmol), aromatic aldehyde (1 mmol), 6-aminouracil (1 mmol), and 0.005 g MWCNTs@L-His/Cu(II) was added to 5 ml of EtOH. The reaction mixture was refluxed for required time (as shown in Table 4) with constant stirring. The progress of the reaction was monitored by thin layer chromatography (TLC). After completion, the reaction mixture was allowed to cool to room temperature. The crude product was dissolved in hot EtOH and filtered for separation of solid catalyst. Evaporation of filtrate gave the pure product. The spectroscopic data of products were reported as followed:

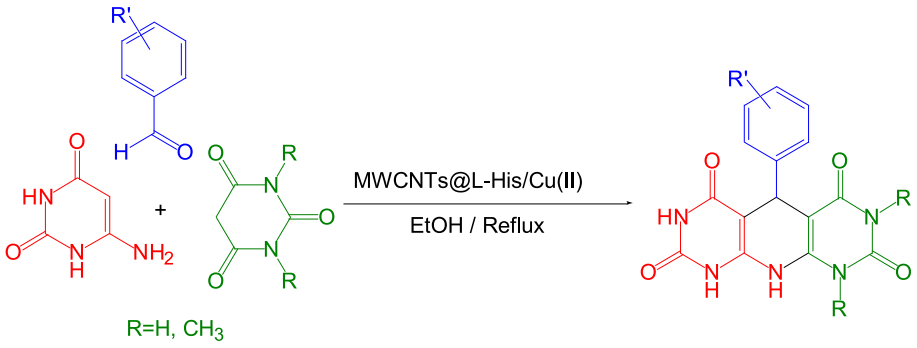

Scheme 1. Synthesis of pyrido[2,3-*d*:5,6-*d'*]dipyrimidine derivatives in the presence of MWCNTs@L-His/Cu(II)

2.3.1. 5-Phenyl-9,10-dihydropyrido[2,3-d:6,5-d']dipyrimidine-2,4,6,8(1H,3H,5H,7H)-tetraone (1)

mp: >300 °C (lit [38].: >300 °C); IR (KBr, cm^{-1}): 3360, 3161, 1706, 1630; ^{1}H NMR (400 MHz, DMSO-d_6): 5.29 (s, 1H, CH), 6.17 (s, 1H, NH), 7.04–7.21 (m, 5H, Ar-H), 10.06 (s, 1H, NH), 10.3 (s, 1H, NH), 10.4 (s, H, NH), 11.07 (s,1H, NH).

2.3.2. 5-(3-nitrophenyl)-9,10-dihydropyrido[2,3-d:6,5-d'] dipyrimidine-2,4,6,8 (1H,3,5H,7H)-tetraone (2)

mp: 249–251 °C (lit [44].: 250 °C); IR (KBr, cm^{-1}): 3457, 3197, 1715, 1629, 1524, 1348; ^{1}H NMR (400 MHz, DMSO-d_6): 5.36 (s, 1H, CH), 6.74 (s, 1H, NH), 7.55 (t, $J = 8$ Hz, 1H, Ar-H), 7.63 (d, 1H, Ar-H), 7.88 (s, 1H, Ar-H), 8.03 (d, $J = 8$ Hz, 1H, Ar-H), 10.93 (s, 1H, NH), 10.98 (s, 1H, NH), 11.18 (s, 1H, NH), 14.30 (s,1H, NH).

2.3.3. 5-(4-nitrophenyl)-9,10-dihydropyrido[2,3-d:6,5-d'] dipyrimidine-2,4,6,8(1H,3H,5H,7H)-tetraone (3)

mp: 218–220 °C (lit [41].: 216–218 °C); IR (KBr, cm^{-1}): 3443, 3162, 1704, 1632, 1514, 1348; ^{1}H NMR (400 MHz, DMSO-d_6): 5.34 (s, 1H, CH), 6.71 (s, 1H, NH), 7.41 (d, $J = 8$ Hz, 2H, Ar-H), 8.09 (d, $J = 8$ Hz, 2H, Ar-H), 10.9 (s, 2H, 2NH), 11.16 (s, 2H, 2NH).

2.3.4. 5-(2-Chlorophenyl)-9,10-dihydropyrido[2,3-d:6,5-d'] dipyrimidine-2,4,6,8(1H,3H,5H,7 H)-tetraone (4)

mp: >300 °C; IR (KBr, cm^{-1}): 3333, 3194, 1710, 1664, 1289, 1076; ^{1}H NMR (400 MHz, DMSO-d_6): 5.27 (s, 1H, CH), 6.55 (s, 1H, NH), 7.19–7.33 (m, 4H, Ar-H), 10.89 (s, 1H, NH), 11.04 (s, 1H, NH), 11.13 (s, 1H, NH), 14.36 (s, 1H, NH); ^{13}C NMR (250 MHz, DMSO-d_6): 167.07, 163.10, 155.41,150.35, 149.59, 138.07, 132.96, 130.26, 128.22, 126.93, 90.70, 87.98, 31.68; Anal. Calcd. for $C_{15}H_{10}ClN_5O_4$: C, 50.08; H, 2.80; Cl, 9.85; N, 19.47; O, 17.79. Found: C, 50.12; H, 2.91; Cl, 9.85; N, 19.37; O, 17.68.

2.3.5. 5-(4-chlorophenyl)-9,10-dihydropyrido[2,3-d:6,5-d'] dipyrimidine-2,4,6,8(1H,3H,5H, 7H)-tetraone (5)

mp: 300–302 °C (lit [44].: 300 °C); IR (KBr, cm^{-1}): 3445, 3163, 1703, 1631, 1290, 1093; ^{1}H NMR (400 MHz, DMSO-d_6): 5.22 (s, 1H, CH), 6.66 (s, 1H, NH), 7.13 (d, $J = 8$ Hz, 2H, Ar-H), 7.27 (d, $J = 8$ Hz, 2H, Ar-H), 10.85 (s, 2H, 2NH), 11.11 (s, 2H, 2NH).

2.3.6. 5-(4-bromophenyl)-9,10-dihydropyrido[2,3-d:6,5-d'] dipyrimidine-2,4,6,8(1H,3H,5H, 7H)-tetraone (6)

mp: >300 °C (lit [45].: >300 °C); IR (KBr, cm^{-1}): 3346, 3153, 1710, 1628, 1145, 1088; ^{1}H NMR (400 MHz, DMSO-d_6): 5.26 (s, 1H, CH), 6.68 (s, 1H, NH), 7.05 (d, $J = 8$ Hz, 2H, Ar-H), 7.22 (d, $J = 8$ Hz, 2H, Ar-H), 10.32 (s, 2H, 2NH), 10.52 (s, 2H, 2NH).

2.3.7. 5-(4-methylphenyl)-9,10-dihydropyrido[2,3-d:6,5-d'] dipyrimidine-2,4,6,8(1H,3H,5H, 7H)-tetraone (7)

mp: >300 °C (lit [44].: >300 °C); IR (KBr, cm^{-1}): 3410, 3198, 1710, 1624; ^{1}H NMR (400 MHz, DMSO-d_6): 2.23 (s, 3H, CH_3), 5.19 (s,1H, CH), 6.62 (s, 1H, NH), 6.93 (d, $J = 8$ Hz, 2H, Ph), 7.02 (d, $J = 8$ Hz, 2H, Ph), 10.48 (s, 1H, 1NH), 10.81 (s, 1H, 1NH), 10.88 (s, 1H, 1NH). 11.06 (s, 1H, 1NH).

2.3.8. 5-(4-methoxyphenyl)-9,10-dihydropyrido[2,3-d:6,5-d'] dipyrimidine-2,4,6,8(1H,3H, 5H,7H)-tetraone (8)

mp: 278–280 °C (lit [41].: 277–278 °C); IR (KBr, cm^{-1}): 3423, 3207, 3071, 1728, 1676; ^{1}H NMR (400 MHz, DMSO-d_6): 3.69 (s, 1H, CH), 3.87 (s, 3H, OCH_3), 7.05 (d, $J = 8$ Hz, 2H, Ph), 8.24 (s, 1H, NH), 8.35 (d, $J = 8$ Hz, 2H, Ph), 11.17 (s, 2H, 2NH), 11.29 (s, 2H, 2NH).

2.3.9. 5-(2-hydroxy-5-nitrophenyl)-9,10-dihydropyrido[2,3-d:6,5-d']dipyrimidine-2,4,6,8 (1H,3H,5H,7H)-tetraone (9)

mp: >300 °C; IR (KBr, cm^{-1}): 3378, 3211, 1724, 1646, 1524, 1335; ^{1}H NMR (400 MHz, DMSO-d_6): 4.92 (s, 1H, CH), 6.59 (s, 1H, OH), 7.2 (s, 1H, NH), 7.22 (s, 1H, NH), 7. 9 (s, 1H, Ph), 8.03 (d, 1H, Ar-H), 8.05 (d, 1H, Ar-H), 10.05 (s, 1H, 1NH), 10.99 (s, 1H, 1NH), 11.89 (s, 1H, 1NH); ^{13}C NMR (250 MHz, DMSO-d_6): 163.60, 163.27, 154.42, 152.11, 150.55, 149.94, 144.25, 126.87, 124.64, 123.70, 116.99, 89.73, 86.74, 27.15; Anal. Calcd. for $C_{17}H_{14}N_6O_6$: C, 51.26; H, 3.54; N, 21.10; O, 24.10. Found: C, 51.36; H, 3.44; N, 21.13; O, 24.21.

2.3.10. 5,5'-(1,4-phenylene)bis(9,10-dihydropyrido[2,3-d:6,5-d'] dipyrimidine-2,4,6,8 (1H,3H,5H,7H)-tetrone) (10)

mp: >300 °C (lit [46].: >300 °C); IR (KBr, cm^{-1}): 3460, 3204, 1706, 1627; ^{1}H NMR (400 MHz, DMSO-d_6): 5.2 (s, 1H, CH), 6.6 (s, 1H, NH), 6.97 (s, 1H, Ar-H), 10.78 (s, 1H, 1NH), 10.86 (s, 1H, 1NH) 11.04 (s, 1H, 1NH), 14.24 (s, 1H, 1NH).

2.3.11. 1,3-Dimethyl-5-phenyl-9,10-dihydropyrido[2,3-d:6,5-d'] dipyrimidine-2,4,6,8 (1H,3H,5H,7H)-tetraone (11)

mp: >300 °C (lit [38].: >300 °C); IR (KBr, cm^{-1}): 3416, 3169, 1736, 1645; ^{1}H NMR (400 MHz, DMSO-d_6): 3.1 (s, 3H, CH_3), 3.19 (s, 3H, CH_3), 4.4 (s, 1H, CH), 6.18 (s, 1H, NH), 6.8–7.2 (5H, m, Ar-H), 10.06 (s, 1H, NH), 10.08 (s, 1H, NH).

2.3.12. 1,3-dimethyl-5-(3-nitrophenyl)-9,10-dihydropyrido[2,3-d:6,5-d']dipyrimidine-2,4,6,8 (1H,3H,5H,7H)-tetraone (12)

mp: >300 °C; IR (KBr, cm^{-1}): 3378, 3204, 1706, 1630, 1524, 1349; ^{1}H NMR (400 MHz, DMSO-d_6): 3.5 (s, 6H, $2CH_3$), 5.49 (s, 1H, CH), 6.90 (s, 1H, NH), 7. 5 (t, $J = 8$ Hz, 2H, Ar-H), 7.7 (s, 1H, Ar-H), 8.01 (d, $J = 8$ Hz, 1H, Ar-H), 11.01 (s, 1H, 1NH), 11.32 (s, 1H, 1NH); ^{13}C NMR (250 MHz, DMSO-d_6): 167.22, 165.82, 156.45, 151.29, 149.61, 148.22, 142.84, 134.42, 129.78, 121.40, 91.14, 86.74, 33.57, 28.68; Anal. Calcd. for $C_{17}H_{14}N_6O_6$: C, 51.26; H, 3.54; N, 21.10; O, 24.10. Found: C, 51.36; H, 3.44; N, 21.13; O, 24.21.

2.3.13. 5-(2-chlorophenyl)-1,3-dimethyl-9,10-dihydropyrido[2,3-d:6,5-d']dipyrimidine-2,4,6,8(1H,3H,5H,7H)-tetraone (13)

mp: >300 °C (lit [43].: mp: >300 °C); IR (KBr, cm^{-1}): 3347, 3206, 1725, 1630, 1236, 1142; ^{1}H NMR (400 MHz, DMSO-d_6): 3.4 (s, 6H, $2CH_3$), 5.24 (s, 1H, CH), 6.48 (s, 1H, NH), 7.2–7.4 (m, 4H, Ar-H), 10.1 (s, 1H, 1NH), 10.9 (s, 1H, 1NH).

2.3.14. 1,3-Dimethyl-5-(4-methylphenyl)-9,10-dihydropyrido[2,3-d:6,5-d']dipyrimidine-2,4,6,8(1H,3H,5H,7H)-tetraone (14)

mp: >300 °C (lit [38].: mp: >300 °C); IR (KBr, cm^{-1}): 3357, 3159, 1707, 1628, 1387; ^{1}H NMR (400 MHz, DMSO-d_6): 2.22 (s, 3H, CH_3), 2.48 (s, 6H, $2CH_3$), 5.2 (s, 1H, CH), 6.7 (s, 1H, NH), 6.93 (d, 2H, Ar-H), 6.98 (d, $J = 8$ Hz, 2H, Ar-H), 10.27 (s, 1H, 1NH), 10.48 (s, 1H, 1NH).

2.3.15. 10-(4-(1,3-dimethyl-2,4,6,8-tetraoxo-1,2,3,4,5,6,7,8,9,10-decahydropyrido[2,3-d:6,5-d']dipyrimidin-5-yl)phenyl)-1,3-dimethyl-5,10-dihydropyrido[3,2-d:5,6-d']dipyrimidine-2,4,6,8(1H,3H,7H,9H)-tetraone (15)

mp: >300 °C; IR (KBr, cm^{-1}): 3352, 3160, 1706, 1628; ^{1}H NMR (400 MHz, DMSO-d_6): 5.23 (s, 1H, CH), 6.63 (s, 1H, NH), 6.87 (s, 2H, Ar-H), 10.25 (s, 1H, NH), 10.45 (s, 1H, NH); ^{13}C NMR (250 MHz, DMSO-d_6): 165.82, 161.00, 150.19, 148.15, 134.18, 129.60, 74.57, 37.21, 32.45, 29.44; Anal. Calcd. for $C_{28}H_{24}N_{10}O_8$: C, 53.50; H, 3.85; N, 22.28; O, 20.36. Found: C, 53.61; H, 3.91; N, 22.19; O, 20.24.

3. Results and discussion

3.1. Characterization of the prepared catalyst

The process for the preparation of MWCNTs@L-His/Cu(II) is schematically described in Scheme 2. At first, MWCNTs were functionalized by L-histidine groups in several steps and then, the

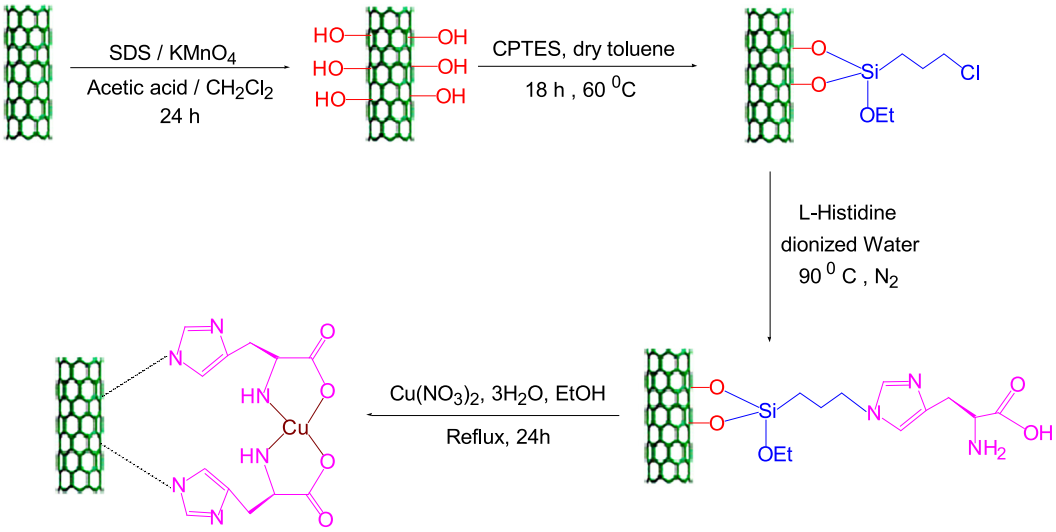

Scheme 2. Preparation of MWCNTs@L-His/Cu(II)

MWCNTs@L-His/Cu(II) was easily prepared by the reaction of MWCNTs@L-His with $Cu(NO_3)_2 \cdot 3H_2O$. After successful preparation of the MWCNTs@L-His/Cu(II), the prepared catalyst was analyzed using Fourier transform infrared (FTIR), thermo-gravimetric analysis (TGA), scanning electron microscopy (SEM), Transmission electron microscopy (TEM), inductively coupled plasma optical emission spectrometry (ICP-OES) and energy-dispersive X-ray spectroscopy (EDS) techniques.

Fig. 1a-e shows the FTIR spectrum of raw MWCNTs, MWCNTs-OH, MWCNT-CPTES, MWCNTs@L-His and MWCNTs@L-His/Cu(II) respectively. The absorption bands of the stretching vibrations of C=C in the structure of raw carbon nanotubes (Fig. 1a), are not observed because the raw nanotubes are totally symmetric and vibrations had the least change in the dipole moment of *C*-C bands. Fig. 1b shows the FTIR spectrum of MWCNTs-OH. The bands observed at 3423 cm^{-1} and 2922 cm^{-1} could be attributed to the stretching vibration of *O*-H and *C*-H respectively. Finally, the C=C and *C*-O vibration bands in the 1633 cm^{-1} and 1112 cm^{-1} region were found in the FTIR spectra of MWCNT-OH. FTIR spectrum of MWCNT-CPTES is shown in Fig .1c. The bands at 1117, 1040 and 691 cm^{-1} assigned to the *Si*-C, *Si*-O and *C*-Cl stretching vibrations respectively. Fig. 1d shows the FTIR spectrum of the MWCNTs@L-His.The absorption bands at 3443 cm^{-1} are from the stretching vibration of *O*-H that recorded together with the *N*-H absorption bands. The peak of bending absorption of carboxylate (COO^-) group appears at 1628 cm^{-1}. The bands appeared at 1108 and 1622 cm^{-1} can be assigned to the vibration of *C*-N and C=N in imidazolium rings, respectively. The infrared spectrum of the MWCNTs@L-His/Cu(II) shows changes in the positions of some bands compare to those of in MWCNTs@L-His, (suggesting the coordination with copper atoms). The carboxylate and amine bands have major changes in this step. The infrared spectrum of the MWCNTs@L-His/Cu(II) complex exhibits Cu-O and Cu-N stretching bands at 974 and 450 cm^{-1}, respectively (Fig. 1e). These results confirm the introduction of carboxylate and nitrogen of amino groups of L-Histidine to Cu(II) ions through coordination mode.

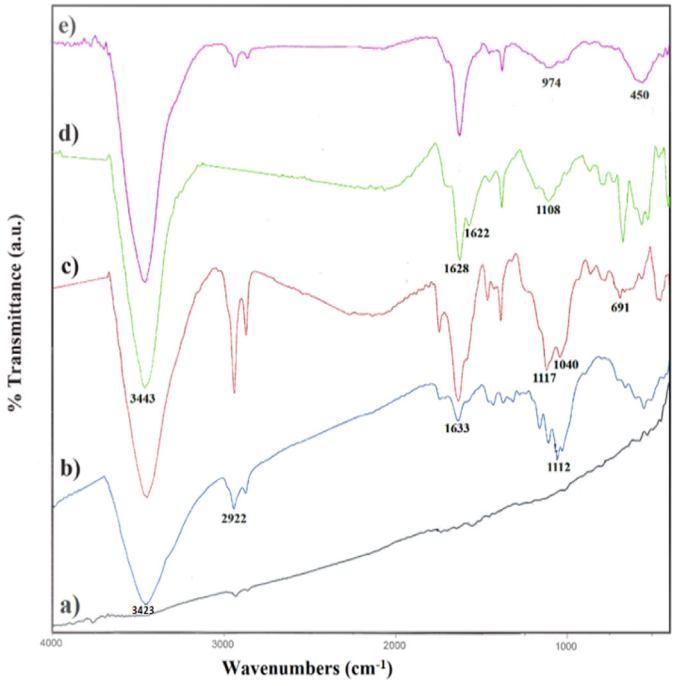

Fig. 1. FT-IR spectra of (a) raw MWCNTs, (b) MWCNTs-OH (c) MWCNTs-CPTES, (d) MWCNTs@L-His, (e) MWCNTs@L-His/Cu(II).

The morphology of pristine MWCNTs and MWCNTs@L-His/Cu(II) were characterized by scanning electron microscopy (SEM) and transmission electron microscopy (TEM) in Fig. 2. The SEM image of raw MWCNTs shows that the tube surfaces are clear and smooth (Fig. 2a). Obviously diameter dimensions of MWCNTs@L-His/Cu(II) are increased, while the length of the nanotubes remained constant (Fig. 2b). All above mentioned changes in morphology demonstrated that the L-His/Cu(II) chemically attached on MWCNTs surfaces. Also TEM images of catalyst (Fig. 2e and f) clearly demonstrate the deposition of Cu on CNT surfaces (black spots) compare with raw MWCNTs with highly pure surfaces (Fig. 2c and d).

The thermal stability of MWCNTs@L-His/Cu(II) was analyzed by Thermogravimetric analysis (TGA), which can be used for quantitative degradation of the sample and estimation of the functionalization percentage of MWCNTs (Fig. 3). Fig. 3a displays the TGA curve of the raw MWCNTs. As can be seen, there is no weight loss between 50 and 800 °C. The weight loss about 5% between 50 and 150 °C was from removal the H_2O absorbed on CNT surfaces; also

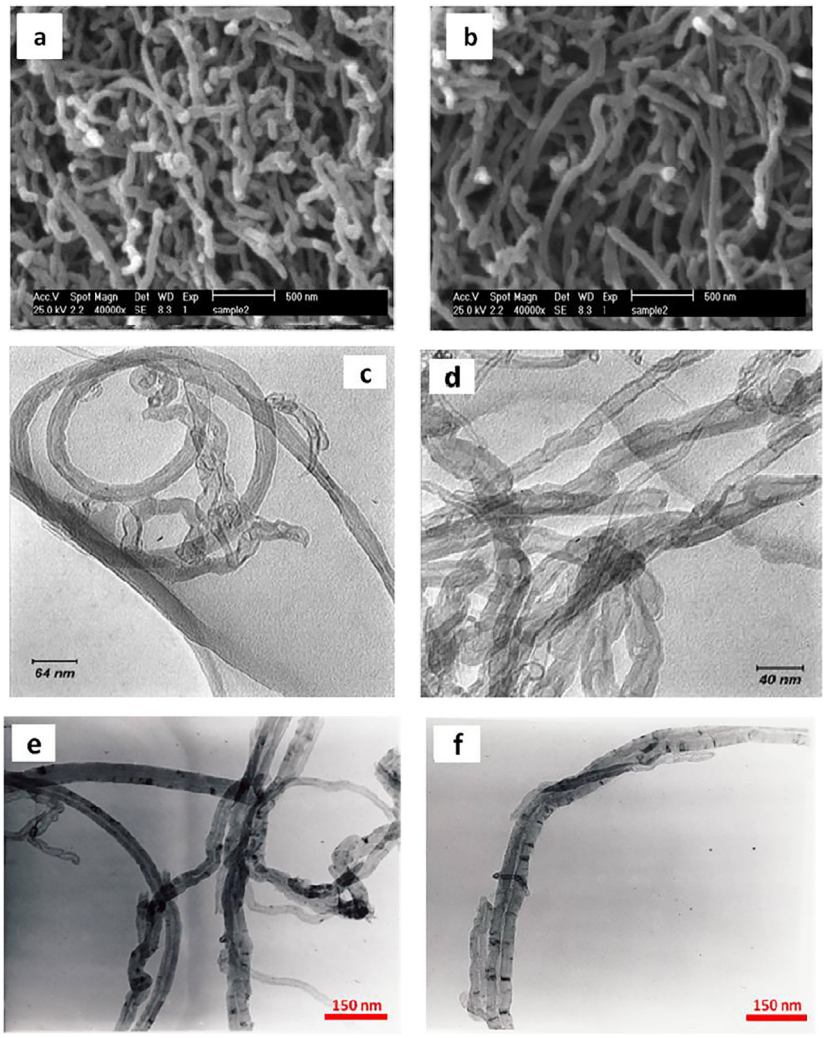

Fig. 2. SEM images of raw MWCNTs (a), MWCNTs@L-His/Cu(II) (b) and TEM images of raw MWCNTs (c, d) and catalyst (e,f).

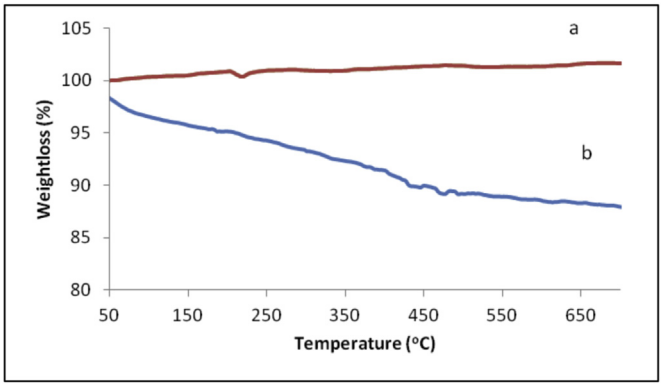

Fig. 3. TGA graph of (a) raw MWCNTs (b) MWCNTs@L-His/Cu(II)

14% weight loss at 150–600 °C in TGA graph of MWCNTs@L-His/Cu(II) is mainly related to the decomposition of covalently bonded organic groups grafted to the MWCNTs surfaces (b in Fig. 3(.

Results from BET analysis (Table 1) show that the functionalization procedure increases the specific surface area of pristine MWCNTs. In fact, functionalization treatment opening up the tube end caps and generates defects on the sidewalls of nanotubes, as well as debundling of CNTs [47–49]. Also total pore volume of catalyst is lower than raw sample due to attachment of L-Histidine@Cu(II) on CNT surfaces. As a result, surface area has been increased after modification and the access to the CNT surfaces and also immobilized organometallic groups was possible easily.

The elemental compositions of the raw MWCNTs and MWCNTs@L-His/Cu(II) were studied by energy dispersive spectroscopy (EDS) (Fig. 4). The results show the presence of C, H, O, N, Si and Cu in the prepared catalyst structure, which confirmed that the L-His/Cu(II) complex was immobilized on MWCNTs surfaces (Fig. 4a). Also, to support the mentioned observation, the MWCNTs@L-His/Cu(II) was subjected to inductively coupled plasma (ICP) analyzer. ICP analysis indicated the presence of Cu in the catalyst and the content of Cu was estimated to be 1.1% W.

3.2. Optimization of reaction conditions

The prepared MWCNTs@L-His/Cu(II) was used as heterogeneous catalysts for the synthesis of pyrido[2,3-d:6,5-d']dipyrimidines *via* the one-pot three-component condensation of barbituric acid (or 1,3-dimethylbarbituric acid), 6-aminouracil and aromatic aldehydes under reflux conditions. To optimize the reaction conditions, barbituric acid, 6-aminouracil and *P*-Clorobenzaldehyde were selected as a model reaction. To determine the optimal solvent, the

Table 1
BET surface area of MWCNTs and MWCNTs@L-His/Cu(II)

Entry	Sample	Surface area(m^2g^{-1})	Total pore volume (cm^3/g)
1	Raw MWCNT	46.68	0.62
2	MWCNTs@L-His/Cu(II)	87.47	0.36

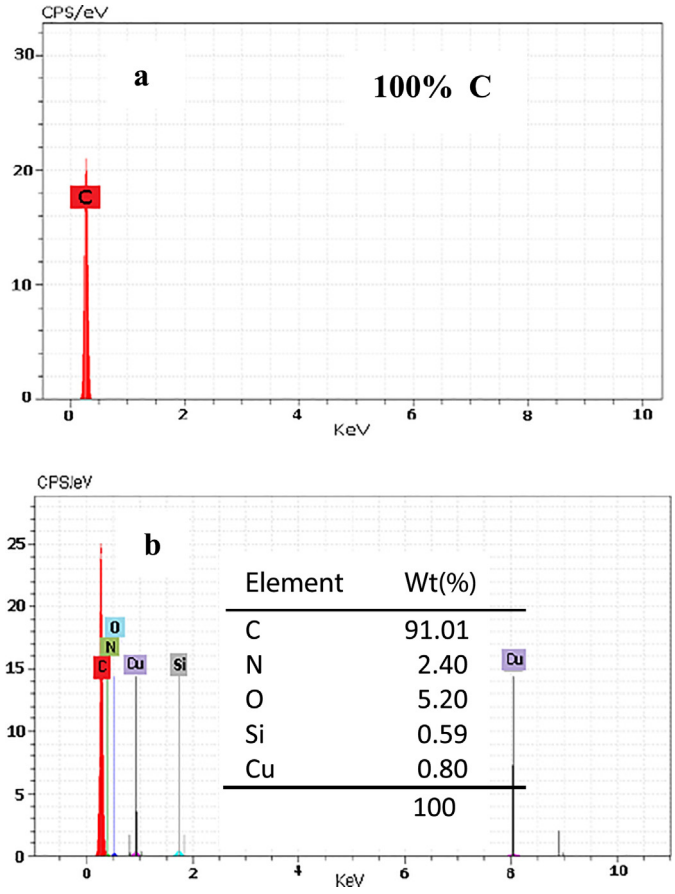

Fig. 4. EDS patterns of (a) raw MWCNTs and (b) MWCNTs@L-His/Cu(II)

reaction was tested in various solvents such as H_2O, EtOH, CH_3CN and DMF in reflux conditions. Also the reaction was tested under solvent-free conditions. As shown in Table 2 (entry 2), the yield of reaction in EtOH and H_2O was more than the other solvents. This outcome shows that polar solvents were better than other solvents (with lower polarity) due to higher solubility of reactants and also more stability of intermediates in EtOH (through the reaction procedure). On the other hand, solvent-free reaction (at 100 °C) caused to decrease the yield of product after long time.

Table 2
Optimization of solvent in synthesis of pyrido[2,3-d:6,5-d']dipyrimidines[a].

Entry	Solvent	Time(min)	Yield[b] (%)
1	H_2O	60	80
2	EtOH	60	95
3	Solvent free[c]	120	60
4	CH_3CN	180	63
5	DMF	180	54

[a] Reaction conditions: barbituric acid (1 mmol), *P*-Clorobenzaldehyde (1 mmol), 6-aminouracil (1 mmol), MWCNTs@L-His/Cu(II) (0.005 g).
[b] Isolated yield.
[c] Temperature: 100 °C.

Table 3
The optimization of MWCNTs@L-His/Cu(II) amount.[a].

Entry	Catalyst (g)	Time (min)	Yield (%)[b]
1	–	120	Trace
2	0.001	120	62
3	0.003	120	80
4	0.005	60	95
5	0.006	60	95
6	0.01	50	95

[a] Reaction conditions: barbituric acid (1 mmol), *P*-Clorobenzaldehyde (1 mmol), 6-aminouracil (1 mmol), in EtOH under reflux conditions.
[b] Isolated yield.

Optimization of catalyst amount was investigated using model reaction in the presence of various amount of catalyst. According to the results depicted in Table 3, the best yield was obtained when 0.005 g of MWCNTs@L-His/Cu(II) was used (entry 4). Increasing the amount of catalyst did not have any effect on the product yield of reaction (entry 5, 6).

In order to determine the optimum temperature, multicomponent reaction was carried out in various temperatures. As can be seen, increasing of the reaction temperature (r.t. to reflux), greatly increased the rate and yield of product (Table 4, entry 5). Therefore, the best result was obtained using 0.005 g of MWCNTs@L-His/Cu(II) as catalyst under reflux conditions to afford the product after 60 min with yield of 95%.

After the optimization of reaction conditions, a series of pyrido[2,3-d:6,5-d']dipyrimidine derivatives were synthesized by the condensation of barbituric acid or 1,3-dimethylbarbituric acid, 6-aminouracil and different aldehydes using MWCNTs@L-His/Cu(II) in optimized conditions (Table 5). As shown in Table 5, the aromatic aldehydes containing electron-withdrawing groups reacted rapidly and gave higher yields, while electron-rich substituted groups on the benzene ring required longer reaction times and got lower yields. Furthermore, the structures of reaction products were supported by ^1H NMR, ^{13}C NMR and FTIR techniques.

Reusability of catalyst was studied for estimation the efficiency and activity of MWCNTs@L-His/Cu(II) in the synthesis of pyrido[2,3-d:5,6-d']dipyrimidine derivatives. After completion of the reaction, the crude product was dissolved in hot EtOH and then the mixture was filtered for removing the solid catalyst. The catalyst was isolated by simple filtration, washed exhaustively with ethanol and distilled water and dried at 85 °C under vacuum for 8 h. Recycled catalyst was used to similar reaction and reused for 6

Table 4
Temperature optimization for the synthesis of pyrido[2,3-d:5,6-d']dipyrimidine derivatives.[a].

Entry	Temperature (°C)	Time(min)	Yield[b] (%)
1	r.t	180	trace
2	40	180	35
3	50	120	60
4	65	120	84
5	78	60	95

[a] Reaction conditions: barbituric acid (1 mmol), *P*-Clorobenzaldehyde (1 mmol), 6-aminouracil (1 mmol), MWCNTs@L-His/Cu(II) (0.005 g) in EtOH.
[b] Isolated yield.

Table 5
Synthesis of pyrido[2,3-d:5,6-d']dipyrimidine derivatives catalyzed by MWCNTs@L-His/Cu(II)[a].

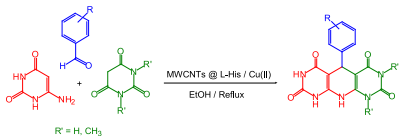

Entry	R′	R	Product	Time (min)	Yield[b] (%)	TON[c]	TOF[d] (min^{-1})
1	H	H	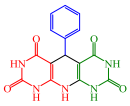	70	92	17,300	14,828
2	H	3-NO_2	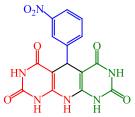	65	93	16,909	15,608
3	H	4-NO_2	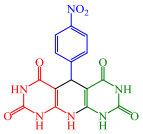	60	93	16,909	16,909
4	H	2-Cl	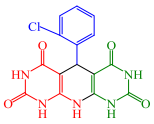	65	90	16,364	15,105
5	H	4-Cl	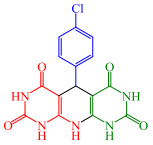	60	95	17,273	17,273
6	H	4-Br	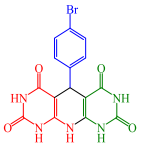	60	91	16,545	16,545
7	H	4-Me	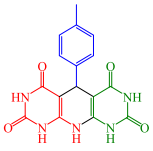	80	85	15,454	11,591
8	H	4-OMe	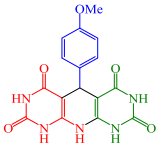	75	89	16,182	12,946
9	H	2-OH, 5-NO_2	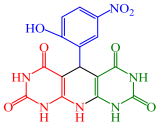	65	90	16,364	15,105

(*continued on next page*)

Table 5 (*continued*)

Entry	R′	R	Product	Time (min)	Yield[b] (%)	TON[c]	TOF[d] (min^{-1})
10	H	4-CHO	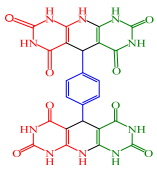	67	91	16,545	14,816
11	CH_3	H	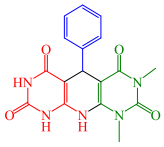	75	80	14,545	11,636
12	CH_3	3-NO_2	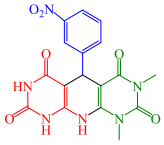	70	83	14,727	12,623
13	CH_3	2-Cl	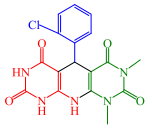	70	82	14,909	12,779
14	CH_3	4-Me	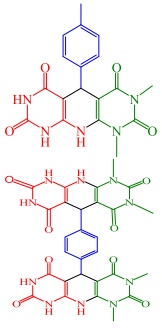	85	78	13,636	9625
15	CH_3	4-CHO		75	80	14,545	11,636

[a] Reaction conditions: barbituric acids (1 mmol), benzaldehyde derivatives (1 mmol), 6-aminouracil (1 mmol), MWCNTs@L-His/Cu(II) (0.005 g) in EtOH under reflux conditions.
[b] Isolated yield.
[c] TON (turn over number): mole of product/mole of catalyst.
[d] TOF (turn over frequency): mol of product/mol of catalyst per min.

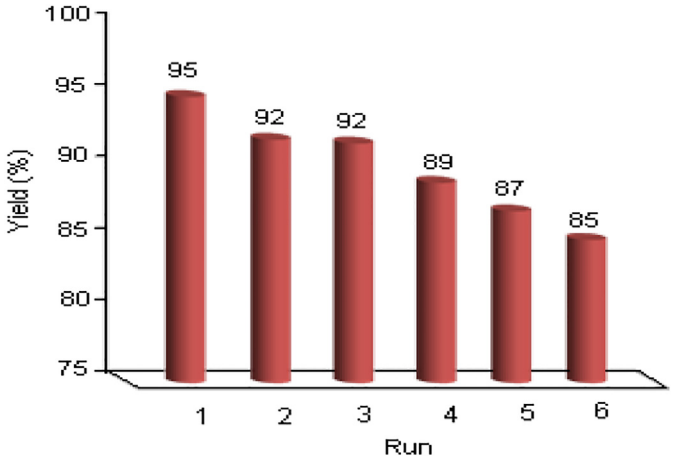

Fig. 5. Reusability of MWCNTs@L-His/Cu(II) in the synthesis of pyrido[2,3-d:6,5-d'] dipyrimidines.

Table 6
Comparison of the catalytic efficiency of MWCNTs@L-His/Cu(II) with other catalysts for the synthesis of dihydropyrido[2,3-d:5,6-d']dipyrimidine.[a].

Entry	Catalyst	Conditions	Time (h)	Yield[b](%)
1	Piperidine	H_2O/60 °C/US	1	87 [34]
2	Triethanolamine	H_2O/80 °C/reflux	3	86 [35]
3	SBA-pr-SO_3H	Solvent free/140 °C	1.5	90 [37]
4	SBA-15-SO_3H	Solvent free/120 °C	0.5	96 [40]
5	$Cu(NO_3)_2$ $3H_2O$	EtOH/reflux	3	44
6	MWCNTs	EtOH/Reflux	10	38
7	MWCNTs@L-Histidine	EtOH/Reflux	5	62
8	MWCNTs@L-His/Cu(II)	EtOH/Reflux	1	92

[a] Reaction conditions for the synthesis of dihydropyrido[2,3-*d*:5,6-*d*′]dipyrimidine-2,4,6,8 (1H, 3H,5H,7H)-tetraone.
[b] Isolated yield.

times (Fig. 5). It was observed that there was no significant loss of catalytic activity of prepared catalyst. In addition, turn over frequency (TOF) and turnover number (TON) values (depicted in Table 5) clearly exhibited high efficiency (due to high turnover

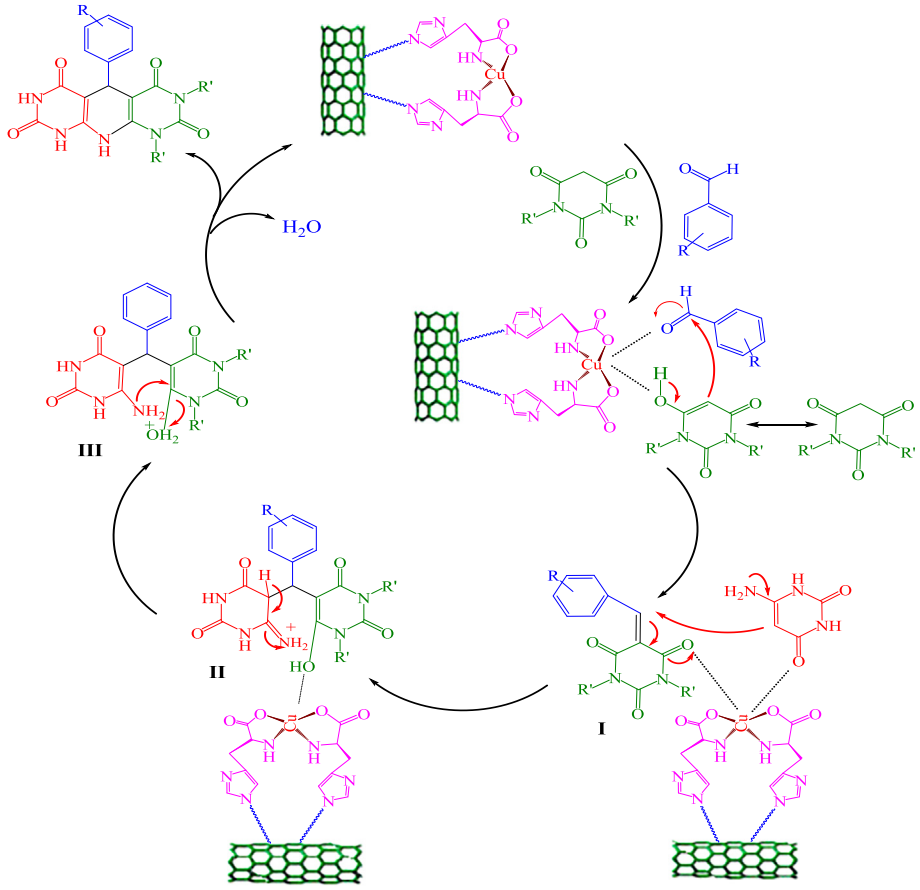

Scheme 3. Proposed mechanism for the synthesis of pyrido[2,3-d:5,6-d']dipyrimidine derivatives.

frequencies) and great stability (high turnover numbers) of synthesized organometallic catalyst.

The results of this study were compared with some literature reports in order to better display the utility of MWCNTs@L-His/Cu(II) in synthesis of pyrido[2,3-*d*:6,5-*d'*]dipyrimidines (Table 6). As can be seen, the MWCNTs@L-His/Cu(II) had some advantages compare with others such as short reaction time with high yield of product, easy workup and reusability of catalyst.

3.3. The proposed reaction mechanism

A plausible mechanism for the synthesis of pyrido[2,3-d:5,6-d'] dipyrimidines catalyzed by MWCNTs@L-His/Cu(II) is shown in Scheme 3. In first step, barbituric acid reacts with aromatic aldehyde in the presence of MWCNTs@L-His/Cu(II) to form standard Knoevenagel condensation product **I**. In fact, Cu(II) as a Lewis acid, can increase the electrophilicity of carbonyl group in aryl aldehyde as well as activation of *C*-H of barbituric acid. After that, the formation of intermediate **II** occurred from Michael-type addition of 6-aminouracil to product **I** in the presence of catalyst. Proton transformation in intermediate **II** resulted the intermediate **III** and Ultimately, after cyclization and water removal from intermediate **III**, pyrido[2,3-d:5,6-d']dipyrimidine derivative was obtained in high yield after short reaction time and releases the catalyst for the next run.

4. Conclusions

In conclusion, we introduced MWCNTs@L-His/Cu(II) catalyst as a highly active heterogeneous catalyst for the synthesis of pyrido [2,3-*d*:5,6-*d'*]dipyrimidine derivatives under reflux conditions. Eventually, this new catalyst has important advantages including easy separation of products, recyclable and reusable without significant loss of activity. Also, high yield of products, short reaction times and the avoidance of toxic organic solvents are some of the important features of this protocol.

Acknowledgements

The authors are grateful to the University of Kashan, for supporting of this work.

References

[1] K. Sun, M.A. Stroscio, M. Dutta, Thermal conductivity of carbon nanotubes, J. Appl. Phys. 105 (2009) 074316–074321.
[2] Z. Han, A. Fina, Z. Han, A. Fina, Thermal conductivity of carbon nanotubes and their polymer nanocomposites: a review, Prog. Polym. Sci. 36 (2011) 914–944.
[3] H. Miyagawa, M. Misra, A.K. Mohanty, Mechanical properties of carbon nanotubes and their polymer nanocomposites, J. Nanosci. Nanotechnol. 5 (2005) 1593–1619.
[4] A.L. Martinez-Hernandez, C. Velasco-Santos, V.M. Castano, Carbon nanotubes composites: processing, grafting and mechanical and thermal properties, Curr. Nanosci. 6 (2010) 12–39.
[5] S.X. Xu, F.Y. Li, R.Z. Wei, Preparation of novel RuB amorphous alloy catalyst supported on carbon nanotubes, Carbon 43 (2005) 861–864.
[6] W. Chen, J. Ji, X. Duan, G. Qian, P. Li, X. Zhou, X. Zhou, D. Chen, W. Yuan, Unique reactivity in Pt/CNT catalyzed hydrolytic dehydrogenation of ammonia borane, Chem. Commun. 50 (2014) 2142–2144.
[7] D.G. Tong, W. Chu, P. Wu, G.F. Gu, L. Zhang, Mesoporous multiwalled carbon nanotubes as supports for monodispersed iron–boron catalysts: improved hydrogen generation from hydrous hydrazine decomposition, J. Mater. Chem.

1 (2013) 359–366.
[8] D.W.H. Fam, A. Palaniappan, A.I.Y. Tok, B. Lied berg, S.M. Moochhala, A review on technological aspects influencing commercialization of carbon nanotube sensors, Sensor. Actuator. B Chem. 157 (2011) 1–7.
[9] H. Zhu, J. Wei, K. Wang, D. Wu, Applications of carbon materials in photovoltaic solar cells, Solar Energy Mater, Sol. Cell. 93 (2009) 1461–1470.
[10] K. Liu, J. Deslippe, F. Xiao, R.B. Capaz, X. Hong, S. Aloni, A. Zettl, W. Wang, X. Bai, S.G. Louie, E. Wang, F. Wang, An atlas of carbon nanotube optical transitions, Nat. Nanotechnol. 7 (2012) 325–329.
[11] P. Serp, E. Castillejos, Catalysis in carbon nanotubes, ChemCatChem 2 (2010) 41–47.
[12] L. Moradi, M. Zare, Ultrasound-promoted green synthesis of 1,4-dihydropyridines using functionalized MWCNTs as a highly efficient heterogeneous catalyst Green, Chem. Lett. Revi. 11 (2018) [197]–[208].
[13] R. Mahinpour, L. Moradi, Z. Zahraei, N. Pahlevanzadeh, New synthetic method for the synthesis of 1,4-dihydropyridine using aminated multiwalled carbon nanotubes as high efficient catalyst and investigation of their antimicrobial properties, J. Saudi Chem. Soc. 22 (2018) 876–885.
[14] A. Kausar, I. Rafique, B. Muhammad, Perspectives of epoxy/graphene oxide composite: significant features and technical applications, Polym. Plast. Technol. Eng. 55 (2016) 704–722.
[15] R.H. Baughman, A.A. Zakhidov, W.A. de Heer, Carbon nanotubes–the route toward applications, Science 29 (7) (2002) 787–792.
[16] N.A. Kabbashi, M.A. Atieh, A. Al-Mamun, M.E. Mirghami, M. Alam, N. Yahya, Kinetic adsorption of application of carbon nanotubes for Pb(II) removal from aqueous solution, J. Environ. Sci. (China) 21 (2009) 539–544.
[17] M.A. Tofighy, T. Mohammadi, Nickel ions removal from water by two different morphologies of induced CNTs in mullite pore channels as adsorptive membrane, Ceram. Int. 41 (2015) 5464–5472.
[18] K. Anitha, S. Namsani, J.K. Singh, Removal of heavy metal ions using a functionalized single-walled carbon nanotube: a molecular dynamics study, J. Phys. Chem. A 119 (2015) 8349–8358.
[19] Y. Li, F. Liu, B. Xia, Q. Du, P. Zhang, D. Wang, Z. Wang, Y. Xia, Removal of copper from aqueous solution by carbon nanotube/calcium alginate composites, J. Hazard Mater. 177 (2010) 876–880.
[20] K. Pillay, E. Cukrowska, N.J. Coville, Multi-walled carbon nanotubes as adsorbents for the removal of parts per billion levels of hexavalent chromium from aqueous solution, J. Hazard Mater. 166 (2009) 1067–1075.
[21] S. Ghasemi, H. Karami, H. Khanezar, Hydrothermal synthesis of lead dioxide/multiwall carbon nanotube nanocomposite and its application in removal of some organic water pollutants, J. Mater. Sci. 49 (2014) 1014–1024.
[22] Y.J. Kuang, Y. Cui, Y.S. Zhang, Y.M. Yu, X.H. Zhang, J.H. Chen, A strategy for the high dispersion of ptru nanoparticles onto carbon nanotubes and their electrocatalytic oxidation of methanol, Chem. Eur J. 18 (2012) 1522–1527.
[23] H. Wang, Z. Zeng, P. Xu, L. Li, G. Zeng, R. Xiao, Z. Tang, D. Huang, L. Tang, C. Lai, D. Jiang, Y. Liu, H. Yi, L. Qin, S. Ye, X. Rena, W. Tanga, Recent progress in covalent organic framework thin films: fabrications, applications and perspectives, Chem. Soc. Rev. 48 (2019) 488–516.
[24] T. Xiong, X. Yuan, H. Wang, Z. Wu, L. Jiang, L. Leng, K. Xi, X. Cao, G. Zeng, Highly efficient removal of diclofenac sodium from medical wastewater by Mg/Al layered double hydroxide-poly(m-phenylenediamine) composite, Chem. Eng. J. 366 (2019) 83–91.
[25] H. Yi, M. Yan, D. Huang, G. Zeng, C. Lai, M. Li, X. Huo, L. Qin, S. Liu, X. Liu, B. Li, H. Wang, M. Shen, Y. Fu, X. Guo, Synergistic effect of artificial enzyme and 2D nano-structured Bi2WO6 for eco-friendly and efficient biomimetic photocatalysis, Appl. Catal. B Environ. 250 (2019) 52–62.
[26] A.L. Jones, M.D. Hulett, C.R. Parish, Histidine-rich glycoprotein: a novel adaptor protein in plasma that modulates the immune, vascular and coagulation systems, Immunol. Cell Biol. 83 (2005) 106–118.
[27] Y. Hu, Q. Wang, C. Zheng, L. Wu, X. Hou, Y. Lv, Recyclable decoration of amine-functionalized magnetic nanoparticles with Ni2+ for determination of histidine by photochemical vapor generation atomic spectrometry, Anal. Chem. 86 (2014) 842–848.
[28] E. Gagelli, H. Kozłowski, D. Valensin, G. Valensin, Copper homeostasis and neurodegenerative disorders (Alzheimer's, prion, and Parkinson's diseases and amyotrophic lateral sclerosis), Chem. Rev. 106 (2006) 1995–2044.
[29] D.A. Ibrahim, A.M. El-Metwally, Design, synthesis, and biological evaluation of novel pyrimidine derivatives as CDK2 inhibitors, Eur. J. Med. Chem. 45 (2010) 1158–1166.
[30] M.J. Aliaga, D.J. Ramon, M. Yus, Impregnated copper on magnetite: an efficient and green catalyst for the multicomponent preparation of propargylamines under solvent free conditions, Org. Biomol. Chem. 8 (2010) 43–46.
[31] A. Kumar, I. Ahmad, B.S. Chhikara, R. Tiwari, D. Mandal, K. Parang, Synthesis of 3-phenylpyrazolopyrimidine-1,2,3-triazole conjugates and evaluation of their Src kinase inhibitory and anticancer activities, Bioorg. Med. Chem. Lett 21 (2011) 1342–1346.
[32] A. Rosowsky, C.E. Mota, S.F. Queener, Synthesis and antifolate activity of 2,4-diamino-5,6,7,8-tetrahydropyrido[4,3-d]pyrimidine analogues of trimetrexate and piritrexim, J. Heterocycl. Chem. 32 (1995) 335–340.
[33] F. Rigueiro, S. Teixeira, A.M. Salaheldin, A.M.F. OliveiraCampos, L.M. Rodrigues, F. Peixoto, M.M. Oliveir, Evaluation of antioxidant properties of some pyrazolo [3,4-d]pyrimidines derivatives and their effects on mitochondria bioenergetics, Biochim. Biophys. Acta 1777 (2008) 62–64.
[34] B.S. Holla, M. Mahalinga, M.S. Karthikeyan, P.M. Akberali, N.S. Shetty, Synthesis of some novel pyrazolo[3,4-d]pyrimidine derivatives as potential antimicrobial agents, Bioorg. Med. Chem. 14 (2006) 2040–2047.
[35] I.O. Donkor, C.L. Klein, L. Liang, N. Zhu, E. Bradley, A.M. Clark, Synthesis and antimicrobial activity of 6,7-annulated pyrido[2,3-d]pyrimidines, J. Pharm. Sci. 84 (1995) 661–664.
[36] M. Bakavoli, G. Bagherzadeh, M. Vaseghifar, A. Shiri, M. Pordel, M. Mashreghi, P. Pordeli, M. Araghi, Molecular iodine promoted synthesis of new pyrazolo [3,4-d]pyrimidine derivatives as potential antibacterial agents, Eur. J. Med. Chem. 45 (2010) 647–650.
[37] J.H. Chern, K.S. Shia, T.A. Hsu, C.L. Tai, C.C. Lee, Y.C. Lee, C.S. Chang, S.N. Tseng, S.R. Shih, Design, synthesis, and structure-activity relationships of pyrazolo [3,4-d]pyrimidines: a novel class of potent enterovirus inhibitors, Bioorg. Med. Chem. Lett 14 (2004) 2519–2525.
[38] M.H. Mosslemin, M.R. Nateghi, Rapid and efficient synthesis of fused heterocyclic pyrimidines under ultrasonic irradiation, Ultrason. Sonochem. 17 (2010) 162–167.
[39] P. Bhattacharyya, S. Paul, A.R. Das, Facile synthesis of pyridopyrimidine and coumarin fused pyridine libraries over a Lewis base-surfactant-combined catalyst TEOA in aqueous medium, RSC Adv. 3 (2013) 3203–3208.
[40] Sh Abdolmohammadi, S. Balalaie, M. Barari, F. Rominger, Three-component green reaction of arylaldehydes, 6-amino-1,3-dimethyluracil and active methylene compounds catalyzed by Zr(HSO4)4 under solvent-free conditions, Comb. Chem. High Throughput Screen 16 (2013) 150–159.
[41] G.M. Ziarani, P. Ghlamzadeh, A. Badiei, S.H. Asadi, A.A. Soorki, Application of SBA-15 functionalized sulfonic acid (SBA-Pr-SO3H) as an efficient nanoreactor in the one-pot synthesis of pyrido[2,3-d]pyrimidine, J. Chil. Chem. Soc. 60 (2015) 2975–2978.
[42] A.M. Abdelmoniem, H.M.E. Hassaneen, I. Abdelshafy Abdelhamid, An efficient one-pot synthesis of novel spiro cyclic 2-oxindole derivatives of pyrimido[4,5-*b*]quinoline, pyrido[2,3-*d*:6,5-*d*′]dipyrimidine and indeno[2′,1′:5,6]pyrido [2,3-*d*]pyrimidine in water, J. Heterocycl. Chem. 53 (2016) 2084–2090.
[43] K.T. Patil, P.P. Warekar, P.T. Patil, S.S. Undare, G.B. Kolekar, P.V. Anbhule, P2O5 mediated an efficient synthesis and biological evaluation of heterocyclic-fused pyrimidine derivatives as an antitubercular agent, J. Heterocycl. Chem. 55 (2018) 154–160.
[44] Sh Rostamizadeh, L. Tahershamsi, N. Zekri, An efficient, one-pot synthesis of pyrido[2,3-d:6,5-d′]dipyrimidines using SBA-15-supported sulfonic acid nanocatalyst under solvent-free conditions, J. Iran. Chem. Soc. 12 (2015) 1381–1389.
[45] N. Azizi, A. Mobinikhaledi, A. Amiri, H. Ghafuri, Catalyst-free synthesis of dihydropyridine from barbituric acid in water, Res. Chem. Intermed. 3 (2012) 2271–2275.
[46] A. Sachar, R.L. Sharma, S. Kumar, D. Kaur, J. Singh, Synthesis of novel bis-condensed heterocyclic ring assembly systems, J. Heterocycl. Chem. 43 (2006) 1177.
[47] F. Pourfayaz, S. Iranpour, O. Shojaei, Effect of acid treatment of carbon nanotubes on their adsorption capacities of benzene and toluene, Int. J. Nanosci. Nanotechnol. 11 (2015) 219–224.
[48] A.A. Farghali, H.A. Abdel Tawab, S.A. Abdel Moaty, Rehab Khaled, Functionalization of acidified multi-walled carbon nanotubes for removal of heavy metals in aqueous solutions, J. Nanostructure Chem. 7 (2017) 101–111.
[49] M. Vesali Naseh, A.A. Khodadadi, Y. Mortazavi, O. Alizadeh Sahraei, F. Pourfayaz, S. Mosadegh Sedghi, Functionalization of carbon nanotubes using nitric acid oxidation and DBD plasma, Int. J. Chem. Biomol. Eng. 2 (2009) 66–68.